SAND2023-10791J

Accurate Calculation of Solvation Properties of Lithium Ions in Nonaqueous Solutions

Daniel L. Vigil[a],* Mark J. Stevens[a], and Amalie L. Frischknecht[a]

[a] *Center for Integrated Nanotechnologies, Sandia National Laboratories, Albuquerque, NM, 87185*

E-mail: dlvigi@sandia.gov

Phone: 505-844-1169

Abstract

We perform all-atom molecular dynamics simulations of lithium triflate in 1,2-dimethoxyethane using six different literature force fields. This system is representative of many experimental studies of lithium salts in solvent and polymers. We show that multiple historically common force fields for lithium ions give qualitatively incorrect results when compared with experiments and quantum chemistry calculations. We illustrate the importance of correctly selecting force field parameters and give recommendations on force field choice for lithium electrolyte applications.

Introduction

Lithium-ion batteries are ubiquitous in our daily lives. These batteries require conductive electrolytes, which are usually composed of organic solvents and sometimes polymers.[1,2] Unfortunately, some of these electrolytes are flammable and can also allow the growth of dendrites that can cause batteries to fail.[3] Polymer electrolytes often reduce flammability and dendrite growth, but are usually less conductive than organic solvents, especially at low temperature.[2] To create better electrolytes for lithium ion (Li^+) conduction, we must understand how Li^+ interacts with and moves through polymers and solvents.

Various experimental techniques such as impedance spectroscopy,[4,5] Raman[6–8] and IR spectroscopy,[9,10] neutron scattering,[11] and NMR[12–16] have given insights about the motion and local environment of Li^+ dissolved in polymers and solvents. These techniques give data that are averaged over many lithiums in a sample that can often be very heterogeneous. It is not usually possible from existing experimental techniques to quantitatively determine the contributions to experimental observations from lithium in different environments. For example, IR and Raman spectra usually contain many overlapping peaks, some of which are due to solvent molecules bound to lithium while other peaks are due to free solvent in a bulk environment. Accurately determining the quantity of each type of molecule from the spectra alone is usually not possible.

Atomistic molecular dynamics (MD) simulations are a complementary technique to the previously listed experiments and can give insights at the level of individual atoms and reveal heterogeneity in a sample.[17,18] MD simulations have already been used to understand trends in Li^+ transference number,[19,20] the effect of different polymer backbones on lithium diffusivity,[21–24] and motion of Li^+ through ionic liquids.[25–27] For the previous example of determining populations of free versus bound solvent molecules in solution it is trivial to count each in an MD simulation.

One key choice in conducting a molecular dynamics simulation is the force field (FF) which determines how atoms interact. For lithium ions in solution there are a multitude of published force fields with fixed charges available. Here, we compare a set of these force fields and find a wide variation in results. These results help determine which FF is best and will aid in the development of Li^+ electrolytes.

Computational Methods

We consider OPLS-style all-atom fixed-charge force fields.[28] This type of force field contains pairwise Lennard-Jones (LJ) and Coulomb interactions, and for polyatomic molecules the FF also includes harmonic bonds, harmonic angles, and dihedral interactions.

To compare the performance of the force fields, we simulated a 1.23 molal solution of lithium trifluoromethanesulfonate (triflate or Tf^-) in 1,2-dimethoxyethane (DME, a.k.a. monoglyme or G1). For Tf^- and DME we use literature values for all force field parameters.[29,30] The force field parameters for Li^+ are discussed in the following section. All simulations contained 500 Li^+ atoms, 500 Tf^- molecules, and 4523 DME molecules.

Starting states were constructed at a density of 0.7 g/mL using a Monte Carlo approach with the software EMC.[31,32] Each solution was equilibrated in an NPT ensemble with a Nosé-Hoover thermostat and barostat at 298 K and 1 atm for at least 20 ns. The density was averaged during the last 5 ns, and the box size was adjusted to attain this average

density. The equilibrated density for each force field is given in Table S1. For all force fields, the equilibrium density yielded a Li^+ concentration of 1 ± 0.01 molar. The system was then equilibrated for 10 ns in an NVT ensemble using a Nosé-Hoover thermostat at 298 K. Data was collected for a subsequent 100 ns.

The equations of motion were integrated using a two-level rRESPA[33] scheme, with a 0.5 fs time step for bonds and a 1 fs time step for angles, pair and electrostatic interactions. Electrostatic interactions were treated with a PPPM method with an accuracy of 10^{-4}. All simulations were conducted using LAMMPS.[34]

Results and Discussion

For Li^+ there are three force field parameters to be determined: the Lennard-Jones diameter (σ) and energy (ϵ), and the atomic charge. Although the lithium ion formally carries a +1 charge, all-atom MD force fields include an implicit partial screening of charges, and it has been shown theoretically and *in silico* that using partially reduced charges is the correct way to model ions with fixed charge.[35–39] There are also a variety of explicitly polarizable force fields available,[40–42] but these have increased computational cost compared to fixed-charge force fields, so we focus solely on determining viable fixed-charge force fields and defer comparison of polarizable force fields to future work.

Notably, many fixed-charge force fields were developed with full charges on ions and did not use charge scaling. Regardless of the charge used in the original parameter set, in this study we follow the electronic continuum model and use a lithium ion charge of +0.78 for all simulations.[37] The partial charges on Tf^- have also been scaled by 0.78 to match the lithium charge. In the SI we compare the results from simulations with full charges for the Li^+ and counter ions to those with charges scaled from 1.0 to 0.78.

We now discuss various force fields that employ different LJ parameters for Li^+. Of the force fields for Li^+ considered in this work, the FF developed by Aqvist[43] is the oldest and

was developed by performing free energy perturbations on ions in SPC and TIP3P water. Aqvist compared the hydration free energy from experiments and the FF to verify accuracy. The OPLS force field parameters were developed in a manner similar to those of Aqvist, but instead used TIP4P water and also tried to optimize the ion-water solvation distance.[44] The Soetens, Millot and Maigret (SMM) force field was developed for lithium ions in ethylene carbonate (EC) and used Hartree-Fock calculations to compute association energies which the FF was parameterized to match.[45] The FF by Wu and Wick was parameterized to match the binding energy of Li^+ with dimethyl ether computed via ab initio simulations.[46] The García-Melgarejo, Alejandre, Núñez-Rojas (GMANR) force field is based on that of Wu-Wick, but with scaled ion charge and LJ radius.[30] The Madrid force field was developed for ions in TIP4P/2005[47] water and was parameterized to fit solution density and other structural data.[48] We choose this set of FFs to study, because some are developed for nonaqueous solutions, which is the focus of our simulations. We note that there are additional Li^+ FFs available, most of which were developed for ions in water.[49,50]

Table 1: Lithium force field parameters, Li^+-ligand association times τ (in ns), and Li^+ and DME diffusion constants D (in $Å^2$/ns)

Name	Year	σ (Å)	ϵ $\left(\frac{\text{kcal}}{\text{mol}}\right)$	$\tau_{\text{DME},1}$	$\tau_{\text{DME},2}$	$\tau_{\text{Tf}^-,1}$	$\tau_{\text{Tf}^-,2}$	D_{Li^+}	D_{DME}
OPLS[44]	2006	2.870	0.0005	-	30.65	-	4.91	41.7	88.7
Aqvist[43]	1990	2.126	0.0183	-	39.17	-	6.40	41.2	89.4
Wu-Wick[46]	2010	1.400	0.4000	4.43	15.33	1.67	14.07	46.5	110.0
SMM[45]	1998	1.460	0.1910	3.59	15.37	1.28	14.57	47.5	112.0
Madrid[48]	2019	1.440	0.1040	3.40	40.09	1.17	31.96	45.7	115.6
GMANR[30]	2020	1.092	0.4000	-	>100	-	>100	49.4	108.7

The force field parameters for Li^+ are given in Table 1 along with quantities to be discussed later. From Table 1 it may seem apparent that some of the FFs are similar and others are quite different just based on the LJ parameters. However, in solution Li^+ is more likely to be interacting with solvent or counterions rather than other lithium ions. For many commonly used solvents for Li^+ salts, such as carbonates and ethers, the solvent oxygen (O) has been shown to coordinate to Li^+. The total pair interaction potential between Li^+ and

a DME oxygen (i.e. LJ plus the electrostatic interaction with ion charges scaled by 0.78) is plotted in Figure 1. The LJ interaction between Li^+ and oxygen uses parameters that are the geometric average of the parameters from the Li^+-Li^+ interaction and the oxygen-oxygen interaction, as is the norm for OPLS-style FFs. The Madrid FF originally did not use this mixing scheme, but rather used fit values for the LJ parameters for interactions between atoms of different types. For the sake of transferability, we use geometric mixing here, even for the Madrid FF.

Figure 1 plots the Li^+-O interaction for the six force fields. The electrostatic attraction between the Li^+ and oxygen completely outweighs the attractive r^6 term in the LJ interaction. Thus all the force fields have similar behavior for $r > 2\,\text{Å}$. The differences between force fields come from the r^{12} term in the LJ potential, which begins to counter the attractive electrostatic term at about $r = 2\,\text{Å}$. The exact value of r at which this occurs varies between force fields. The position and depth of the local minimum is set by the length scale at which the r^{12} repulsion counters the attractive electrostatics and is controlled by the combined parameter $\epsilon\sigma^{12}$. This is why the depth and distance of the Li^+-O energy minimum are correlated in Figure 1.

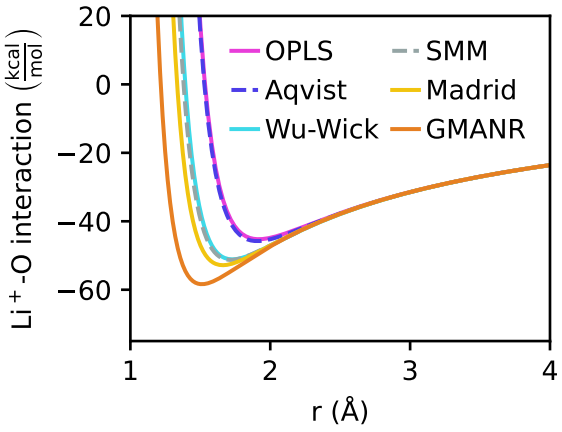

Figure 1: Total pair interaction between Li^+ and DME oxygen.

The energies at the local minimums in Figure 1 are large, on the order of 50 kcal/mol, compared to the thermal energy of 0.6 kcal/mol at 298 K. The potential is for a Li^+ and

oxygen in vacuum so the Coulomb interaction is unscreened and strong. In solution, dielectric screening can reduce the interaction strength at large distances. The difference in energy between two configurations determines the thermodynamic transition between the states and these energies in solution are smaller than the energy to separate a Li^+ and an oxygen in vacuum. Thus the energy for a Li^+ to change association from one oxygen to another is much less than that indicated by the minimum in the potential.

Molecular dynamics simulations of 1M solutions of LiTf in DME were performed using the different force fields listed in Table 1. The simulations yield substantially different local solvation structures for Li^+, which is one of the base criteria for a good parameterization and clearly indicates that some of the FFs are not viable for this system. The radial distribution functions (RDFs) between Li^+ and all other elements are presented in Figure S1. For all force fields considered, Li^+ is surrounded by a primary solvation shell of oxygens. We examine the first oxygen solvation shell in Figure 2, which shows the $g_{Li^+,O}(r)$ RDF as well as the neighborship ordered peaks underlying the RDF.[51] The average number of oxygens in the first solvation shell is also listed in the figure. This number was determined by integrating the RDF up to its first local minimum.

The Aqvist and OPLS FFs have approximately six oxygens coordinating the Li^+ and also have the largest Li^+ LJ radius of all FFs considered. The GMANR FF only has 4 oxygens in the primary solvation shell, and has the smallest Li^+ LJ radius. The three other FFs (SMM, Wu-Wick, Madrid) all have 4-5 oxygens in their first solvation shell and also have intermediate LJ radii. Changing the Li^+ LJ radius can clearly lead to qualitative differences in simulation results.

Various experiments including electrospray ionization mass spectrometry (ESI-MS),[52,53] time-of-flight neutron diffraction,[11] IR spectroscopy,[9,10] Raman spectroscopy,[6–8] and NMR[12–14] have been used to estimate the number of solvent or anion atoms that coordinate lithium in non-aqueous solution at intermediate concentration. Unfortunately there is not a consensus value for the Li^+ coordination number and values in the range 4-6 have been reported.

The Li^+ coordination number has also been calculated with *ab initio* quantum chemistry methods.[14,42,54–58] DFT calculations for Li^+ in water and carbonates find the most optimal coordination of Li^+ by oxygen is 4.[59–61]

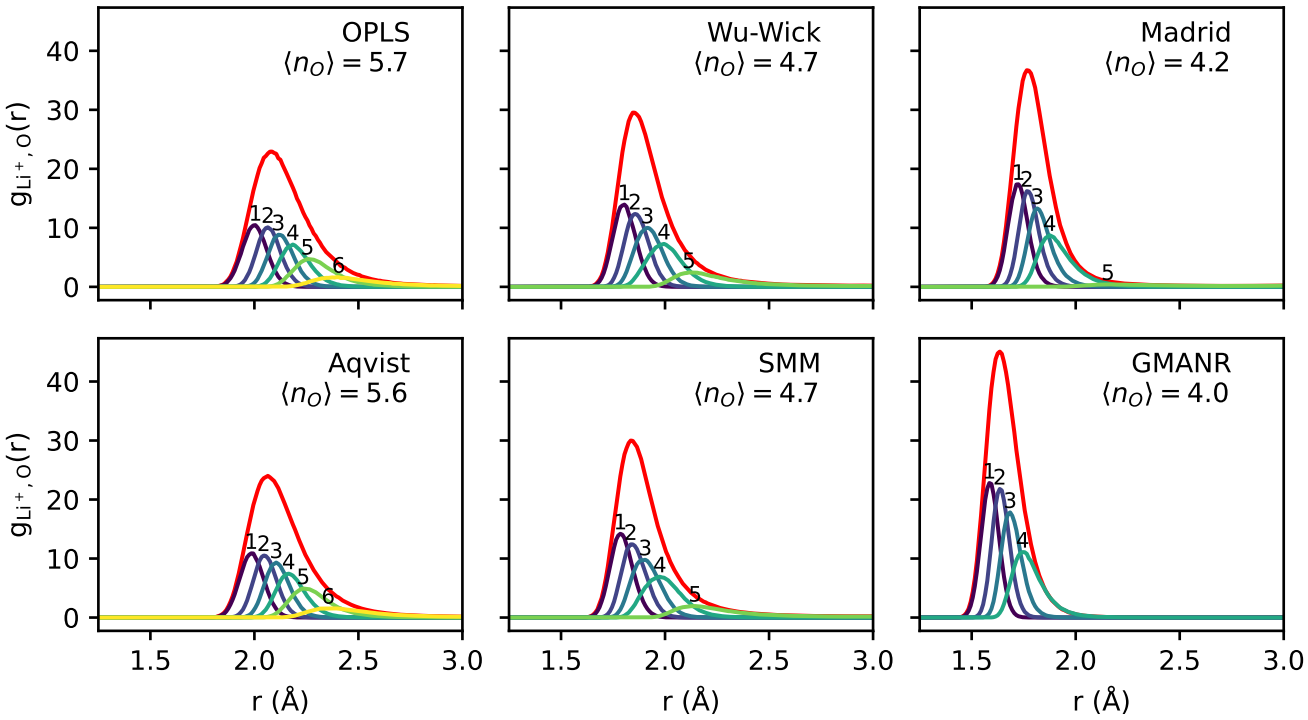

Figure 2: Radial distribution function between Li^+ and oxygen (red) and neighborship-ordered radial distribution functions (numbered curves). Average oxygen number $\langle n_O \rangle$ in the first solvation shell is indicated with text.

Figure 3 shows characteristic snapshots of Li^+ and the coordinating oxygens and molecules for various FFs. Figure 3a shows that the 6-coordinated Li^+ from the OPLS FF tends to form an octahedral arrangement and Figure 3b shows that these oxygens belong to DME molecules that are bidentate coordinated to the Li^+. A similar configuration of bidentate DME around the Li^+ is observed in Figure 3f for the GMANR FF, but with only two DME molecules. These oxygens form a tetrahedral arrangement around the Li^+ as shown in Figure 3e. For the SMM FF, the Li^+ is coordinated by 5 oxygens in a distorted square pyramid structure. Four of the oxygens are part of bidentate DMEs that coordinate the Li, while the fifth oxygen belongs to a Tf^- counter ion that also coordinates to the Li^+. Tetrahedrally

coordinated Li^+ were also observed in simulations with the SMM FF, so the average number of coordinating oxygens $\langle n_0 \rangle = 4.7$ reflects a mix of Li^+ with four or five oxygens in the solvation shell.

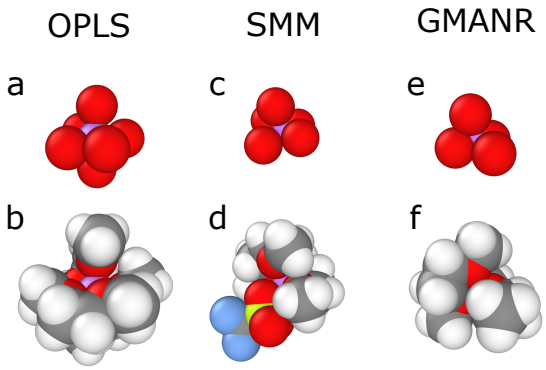

Figure 3: Snapshots of Li^+ coordinated by oxygen (top row) and full molecules (bottom row) in the first solvation shell. Atoms are color coded: Li^+ (purple), oxygen (red), carbon (grey), sulfur (yellow), hydrogen (white), and fluorine (blue).

These differences between FFs can be further quantified by comparing the fraction of Li^+ that are coordinated to a counterion versus completely solvated. We classify the Li^+ into three types of environments: solvated ions, close ion pairs (CIPs), and aggregates. A solvated Li^+ is completely coordinated by solvent (in this case DME), such as in Figure 3b and f. A CIP consists of a pair of Li^+ and Tf^- with at most 3 Å separation between the Li^+ and a Tf^- oxygen atom and that are otherwise completely surrounded by solvent. An aggregate is an assembly of three or more ions with the same Li^+-oxygen separation criteria as CIPs. Aggregates can consist of one Li^+ and two Tf^-, two Li^+ and one Tf^-, or any other higher order product. The fraction of Li^+ that participate in each type of coordination environment is shown in Figure 4. Again we find that the choice of FF substantially affects a structural property of the system.

The Aqvist, OPLS, and GMANR FFs, which result in an even coordination number for Li^+, form mostly solvated Li^+. In contrast, the SMM, Wu-Wick, and Madrids FFs, which result in 4-5 oxygen neighbors coordinating Li^+, form mostly CIPs and aggregates. This is because two bidentate DME molecules do not form a complete solvation shell. A third DME

would only be able to form a monodentate association, which we conjecture is less stable than a monodentate Li^+-Tf^- association. Thus it is favorable to form Li^+-Tf^- associations which leads to mostly CIPs and aggregates in solution.

Raman and IR spectroscopy indicate that LiTf in DME mostly forms CIPs and aggregates.[62–65] Recent simulations using quantum chemistry calculations and atomistic MD simulations also indicate that triflate has a strong association with Li^+ and is expected to form stable ion pairs.[66] The SMM, Wu-Wick, and Madrid FFs form mostly CIPs and aggregates while the other force fields favor solvated ions; therefore, the SMM, Wu-Wick, and Madrid FFs better match the experiments.

The difference in amount and type of CIPs and aggregates formed can be important to electrolyte properties. CIPs in principle do not contribute to conductivity because they are net neutral. Similarly, aggregates can conduct Li^+ if they have a net-positive charge, be non-conducting if they are net-neutral, or be anti-conductive for Li^+ if they have a net-negative charge.[19,67] In practice, the lifetime of associations between ions is also important to conductivity, as ions can attach or detach from aggregates. We now turn to this issue of dynamics.

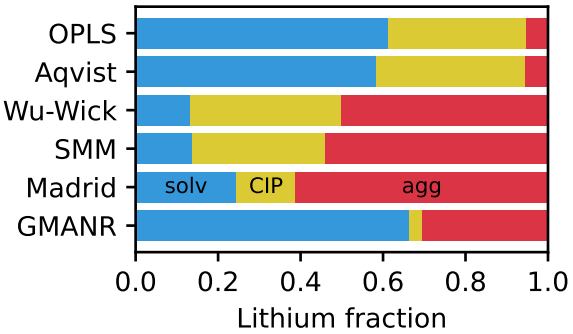

Figure 4: Fraction of lithium ions that are fully solvated (solv, blue), in a close ion pair (CIP, yellow) or are in an aggregate (agg, red).

We first evaluate the Li^+-DME association lifetime and Li^+-Tf^- association lifetime by fitting the intermittent association correlation functions[68–71] to double exponential functions and extracting relaxation times, which are listed in Table 1. Most entries have two relaxation

times τ, because their association curves exhibit two separate time scales for the dissociation of solvent from Li^+. This behavior is perhaps due to the bidentate association of DME with Li^+. For the OPLS and Aqvist FFs, a single exponential was sufficient so only one time scale is listed. For the GMANR FF, the association time was too long to reliably fit from the 100 ns simulations. Figures S3 and S4 show the plots of the intermittent association function between Li^+ and DME oxygens and Li^+ and the Tf^- sulfur, respectively.

The association time between Li^+ and Tf^- is shortest for the OPLS and Aqvist FFs, which have the weakest interaction between Li^+ and oxygen. For the FFs with stronger Li^+-O interactions, the Li^+-Tf^- association time is longer. Figure S5 plots the association times against the Li^+-O interaction minimum energy. The Li^+-Tf^- association time follows a clear monotonic trend with more negative interaction energy corresponding to longer association times.

The Li^+-DME association does not follow a monotonic trend, however. In particular, the Li^+-DME associations last six times longer than the Li^+-Tf^- association for the Aqvist and OPLS FFs, whereas for the SMM, Wu-Wick, and Madrid FFs, the Li^+-DME association is at most 25% longer than the Li^+-Tf^- association. We speculate that for the Aqvist and OPLS FFs the solvation shell of three bidentate DMEs around Li^+ confers extra stability, which leads to longer Li^+-DME associations than Li^+-Tf^-. For the SMM, Wu-Wick, and Madrid FFs the solvation shell is more heterogeneous as seen in Figure 3 and there is no extra stability for DME in the solvation shell.

Table 1 also lists the diffusion coefficients of Li^+ and DME for each force field. The force field parameters used in this study for pure DME lead to a lower DME diffusivity (215 $Å^2$/ns) than that measured in experiments (315 $Å^2$/ns).[15] Consequently, the diffusivities of ions in solution are also lower than those measured experimentally. Nevertheless we can still make comparisons between the force fields.

For all FFs the lifetime of Li^+-O associations is long enough that vehicular motion of Li^+ with its shell of solvent (and possibly counterions) is the dominant transport mode. The FF

with the highest Li^+ diffusivity is GMANR, which is somewhat surprising given that it leads to the longest association times, but the solvation shell is the smallest for GMANR. Given a diffusion mechanism of solvation shell motion, the smallest shell will diffuse fastest according to Stokes-Einstein theory. The Aqvist and OPLS FFs yield the lowest diffusivity for both Li^+ and DME. We attribute this to the large solvation shell around the Li^+ for these FFs.

Additionally, the DME molecules bound to Li^+ cannot move as quickly as free DME in bulk solvent, which depresses the diffusivity for DME in solution. NMR experiments have measured the diffusion constant of pure DME and DME in a 1M LiTf solution.[15,16] The ratio of solution diffusion constant to pure diffusion constant $D_{\mathrm{DME,sol}}/D_{\mathrm{DME,pure}}$ is 0.51. The SMM, Wu-Wick, Madrid, and GMANR FFs all yield values of $D_{\mathrm{DME,sol}}/D_{\mathrm{DME,pure}}$ in the range 0.51 to 0.54, which is good agreement with experiments. The Aqvist and OPLS FFs on the other hand yield a value of $D_{\mathrm{DME,sol}}/D_{\mathrm{DME,pure}} \approx 0.4$, which represents a significant devation from experiments. We remind the reader that only the Li^+ LJ parameters have changed when comparing FFs, not any parameter related to DME, so the differences in $D_{\mathrm{DME,sol}}/D_{\mathrm{DME,pure}}$ between FFs comes from the interactions of DME with Li^+.

Conclusions

We have shown that only changing the Lennard-Jones parameters for Li^+ yields strong variations in the structure and dynamics for a nonaqueous solvent. Thus, care must be taken in choosing force-field parameters for ions even within a fixed charged force field. Of the force fields considered here, the Aqvist and OPLS models overestimate the degree of lithium solvation in DME and underestimate the transport rate. The GMANR force field appears to underestimate the degree of solute pairing and ion aggregation. The remaining three FFs, SMM, Wu-Wick, and Madrid, produce similar results and are in reasonable agreement with experiments with regard to solvation structure, ion pairing and aggregation, and Li^+ dynamics. We encourage future simulators to employ one of these FFs and make

careful consideration of other FF parameters in the future.

Acknowledgement

This work was performed at the Center for Integrated Nanotechnologies, an Office of Science User Facility operated for the U. S. Department of Energy (DOE) Office of Science. Sandia National Laboratories is a multimission laboratory managed and operated by the National Technology and Engineering Solutions of Sandia, LLC, a wholly owned subsidiary of Honeywell International, Inc., for the U.S. Department of Energy's National Nuclear Security Administration under contract DE-NA-0003525. The views expressed in the article do not necessarily represent the views of the U.S. DOE or the United States Government.

Supporting Information Available

Equilibrium densities, pair correlation functions, aggregate size distributions, intermittent association correlation functions, mean square displacements

References

(1) Armand, M. The history of polymer electrolytes. Solid State Ionics **1994**, 69, 309–319.

(2) Zhang, H.; Li, C.; Piszcz, M.; Coya, E.; Rojo, T.; Rodriguez-Martinez, L. M.; Armand, M.; Zhou, Z. Single lithium-ion conducting solid polymer electrolytes: advances and perspectives. Chem. Soc. Rev. **2017**, 46, 797–815.

(3) Armand, M.; Tarascon, J.-M. Building better batteries. Nature **2008**, 451, 652–657.

(4) Evans, J.; Vincent, C. A.; Bruce, P. G. Electrochemical measurement of transference numbers in polymer electrolytes. Polymer **1987**, 28, 2324–2328.

(5) Klein, R. J.; Zhang, S.; Dou, S.; Jones, B. H.; Colby, R. H.; Runt, J. Modeling electrode polarization in dielectric spectroscopy: Ion mobility and mobile ion concentration of single-ion polymer electrolytes. The Journal of Chemical Physics **2006**, 124, 144903.

(6) Baum, R. G.; Popov, A. I. Spectroscopic studies of ionic solvation. XVIII. Solvation of the lithium ion in acetone and acetone-nitromethane mixtures. J. Solution Chem. **1975**, 4, 441–445.

(7) Hyodo, S.-A.; Okabayashi, K. Raman intensity study of local structure in non-aqueous electrolyte solutions—I. Cation-solvent interaction in LiClO4/ethylene carbonate. Electrochim. Acta **1989**, 34, 1551–1556.

(8) Morita, M.; Asai, Y.; Yoshimoto, N.; Ishikawa, M. A Raman spectroscopic study of organic electrolyte solutions based on binary solvent systems of ethylene carbonate with low viscosity solvents which dissolve different lithium salts. J. Chem. Soc., Faraday Trans. **1998**, 94, 3451–3456.

(9) Seo, D. M.; Reininger, S.; Kutcher, M.; Redmond, K.; Euler, W. B.; Lucht, B. L. Role of mixed solvation and ion pairing in the solution structure of lithium ion battery electrolytes. J. Phys. Chem. C **2015**, 119, 14038–14046.

(10) Lim, J.; Lee, K.-K.; Liang, C.; Park, K.-H.; Kim, M.; Kwak, K.; Cho, M. Two-dimensional infrared spectroscopy and molecular dynamics simulation studies of non-aqueous lithium ion battery electrolytes. J. Phys. Chem. B **2019**, 123, 6651–6663, PMID: 31074985.

(11) Kameda, Y.; Umebayashi, Y.; Takeuchi, M.; Wahab, M. A.; Fukuda, S.; Ishiguro, S.-i.; Sasaki, M.; Amo, Y.; Usuki, T. Solvation structure of Li+ in concentrated LiPF6-propylene carbonate solutions. J. Phys. Chem. B **2007**, 111, 6104–6109, PMID: 17497919.

(12) Chan, L. L.; Wong, K.; Smid, J. Complexation of lithium, sodium, and potassium carbanion pairs with polyglycol dimethyl ethers (glymes). Effect of chain length and temperature. J. Am. Chem. Soc. **1970**, 92, 1955–1963.

(13) Kondo, K.; Sano, M.; Hiwara, A.; Omi, T.; Fujita, M.; Kuwae, A.; Iida, M.; Mogi, K.; Yokoyama, H. Conductivity and solvation of Li+ ions of LiPF6 in propylene carbonate solutions. J. Phys. Chem. B **2000**, 104, 5040–5044.

(14) Wan, C.; Hu, M. Y.; Borodin, O.; Qian, J.; Qin, Z.; Zhang, J.-G.; Hu, J. Z. Natural abundance 17O, 6Li NMR and molecular modeling studies of the solvation structures of lithium bis(fluorosulfonyl)imide/1,2-dimethoxyethane liquid electrolytes. J. Power Sources **2016**, 307, 231–243.

(15) Hayamizu, K.; Aihara, Y.; Arai, S.; Martinez, C. G. Pulse-gradient spin-echo 1H, 7Li, and 19F NMR diffusion and ionic conductivity measurements of 14 organic electrolytes containing LiN(SO2CF3)2. J. Phys. Chem. B **1999**, 103, 519–524, PMID: 26251969.

(16) Horwitz, G.; Rodríguez, C.; Factorovich, M.; Corti, H. R. Maximum electrical conductivity of associated lithium salts in solvents for lithium–air batteries. J. Phys. Chem. C **2019**, 123, 12081–12087.

(17) Bolintineanu, D.; Stevens, M. J.; Frischknecht, A. Atomistic simualtions predict a surprising variety of morphologies in precise ionomers. ACS Macro Lett. **2013**, 2, 206.

(18) Bolintineanu, D.; Stevens, M. J.; Frischknecht, A. Influence of cation type on ionic aggregates in precise ionomers. Macromolecules **2013**, 46, 5381.

(19) Molinari, N.; Mailoa, J. P.; Kozinsky, B. General trend of a negative Li effective charge in ionic liquid electrolytes. J. Phys. Chem. Lett. **2019**, 10, 2313–2319.

(20) Fong, K. D.; Self, J.; Diederichsen, K. M.; Wood, B. M.; McCloskey, B. D.; Pers-

son, K. A. Ion transport and the true transference number in nonaqueous polyelectrolyte solutions for lithium ion batteries. ACS Cent. Sci. **2019**, 5, 1250–1260.

(21) Trigg, E. B.; Stevens, M. J.; Winey, K. I. Chain folding produces a multilayered morphology in a precise polymer: simulations and experiments. J. Am. Chem. Soc. **2017**, 139, 3747–3755.

(22) Wheatle, B. K.; Keith, J. R.; Mogurampelly, S.; Lynd, N. A.; Ganesan, V. Influence of dielectric constant on ionic transport in polyether-based electrolytes. ACS Macro Lett. **2017**, 6, 1362–1367, PMID: 35650818.

(23) Savoie, B. M.; Webb, M. A.; Miller, T. F. I. Enhancing cation diffusion and suppressing anion diffusion via Lewis-acidic polymer electrolytes. J. Phys. Chem. Lett. **2017**, 8, 641–646, PMID: 28075599.

(24) Paren, B.; Thurston, B.; Neary, W.; Kendrick, A.; Kennemur, J.; Stevens, M. J.; Frischknecht, A.; Winey, K. Percolated ionic aggregate morphologies and decoupled ion transport in precise sulfonated polymers synthesized by ring-opening metathesis polymerization. Macromolecules **2020**, 53, 8960.

(25) Chen, F.; Pringle, J. M.; Forsyth, M. Insights into the transport of alkali metal ions doped into a plastic crystal electrolyte. Chem. Mater. **2015**, 27, 2666–2672.

(26) Shimizu, K.; Freitas, A. A.; Atkin, R.; Warr, G. G.; FitzGerald, P. A.; Doi, H.; Saito, S.; Ueno, K.; Umebayashi, Y.; Watanabe, M. et al. Structural and aggregate analyses of (Li salt + glyme) mixtures: the complex nature of solvate ionic liquids. Phys. Chem. Chem. Phys. **2015**, 17, 22321–22335.

(27) Thum, A.; Heuer, A.; Shimizu, K.; Canongia Lopes, J. N. Solvate ionic liquids based on lithium bis(trifluoromethanesulfonyl)imide–glyme systems: coordination in MD simulations with scaled charges. Phys. Chem. Chem. Phys. **2020**, 22, 525–535.

(28) Kaminski, G.; Duffy, E. M.; Matsui, T.; Jorgensen, W. L. Free energies of hydration and pure liquid properties of hydrocarbons from the OPLS all-atom model. J. Phys. Chem. **1994**, 98, 13077–13082.

(29) Canongia Lopes, J. N.; Pádua, A. A. H. Molecular force field for ionic liquids composed of triflate or bistriflylimide anions. J. Phys. Chem. B **2004**, 108, 16893–16898.

(30) Garcia-Melgarejo, V.; Alejandre, J.; Núñez-Rojas, E. Parametrization with explicit water of solvents used in lithium-ion batteries: cyclic carbonates and linear ethers. J. Phys. Chem. B **2020**, 124, 4741–4750, PMID: 32425045.

(31) in 't Veld, P. J.; Rutledge, G. C. Temperature-dependent elasticity of a semicrystalline interphase composed of freely rotating chains. Macromolecules **2003**, 36, 7358–7365.

(32) in 't Veld, P. J. EMC: Enhanced Monte Carlo. `https://montecarlo.sourceforge.net/emc/`, Accessed: 2022-10-01.

(33) Tuckerman, M.; Berne, B. J.; Martyna, G. J. Reversible multiple time scale molecular dynamics. J. Chem. Phys. **1992**, 97, 1990–2001.

(34) Thompson, A. P.; Aktulga, H. M.; Berger, R.; Bolintineanu, D. S.; Brown, W. M.; Crozier, P. S.; in 't Veld, P. J.; Kohlmeyer, A.; Moore, S. G.; Nguyen, T. D. et al. LAMMPS - a flexible simulation tool for particle-based materials modeling at the atomic, meso, and continuum scales. Comp. Phys. Comm. **2022**, 271, 108171.

(35) Youngs, T. G. A.; Hardacre, C. Application of static charge transfer within an ionic-liquid force ield and its effect on structure and dynamics. ChemPhysChem **2008**, 9, 1548–1558.

(36) Chaban, V. Polarizability versus mobility: atomistic force field for ionic liquids. Phys. Chem. Chem. Phys. **2011**, 13, 16055–16062.

(37) Leontyev, I.; Stuchebrukhov, A. Accounting for electronic polarization in non-polarizable force fields. Phys. Chem. Chem. Phys. **2011**, 13, 2613–2626.

(38) Leontyev, I. V.; Stuchebrukhov, A. A. Polarizable molecular interactions in condensed phase and their equivalent nonpolarizable models. J. Chem. Phys. **2014**, 141, 014103.

(39) Doherty, B.; Zhong, X.; Gathiaka, S.; Li, B.; Acevedo, O. Revisiting OPLS force field parameters for ionic liquid simulations. J. Chem. Theory Comput. **2017**, 13, 6131–6145, PMID: 29112809.

(40) Dang, L. X. Development of nonadditive intermolecular potentials using molecular dynamics: Solvation of Li+ and F- ions in polarizable water. J. Chem. Phys. **1992**, 96, 6970–6977.

(41) Borodin, O.; Smith, G. D. Development of many-body polarizable force fields for Li-battery applications: 2. LiTFSI-doped oligoether, polyether, and carbonate-based electrolytes. J. Phys. Chem. B **2006**, 110, 6293–6299, PMID: 16553447.

(42) Liyana-Arachchi, T. P.; Haskins, J. B.; Burke, C. M.; Diederichsen, K. M.; McCloskey, B. D.; Lawson, J. W. Polarizable molecular dynamics and experiments of 1,2-dimethoxyethane electrolytes with lithium and sodium salts: structure and transport properties. J. Phys. Chem. B **2018**, 122, 8548–8559, PMID: 30130409.

(43) Aqvist, J. Ion-water interaction potentials derived from free energy perturbation simulations. J. Phys. Chem. **1990**, 94, 8021–8024.

(44) Jensen, K. P.; Jorgensen, W. L. Halide, ammonium, and alkali metal ion parameters for modeling aqueous solutions. J. Chem. Theory and Comput. **2006**, 2, 1499–1509, PMID: 26627020.

(45) Soetens, J.-C.; Millot, C.; Maigret, B. Molecular dynamics simulation of Li+ BF4- in

ethylene carbonate, propylene carbonate, and dimethyl carbonate solvents. J. Phys. Chem. A **1998**, 102, 1055–1061.

(46) Wu, H.; Wick, C. D. Computational investigation on the role of plasticizers on ion conductivity in poly(ethylene oxide) LiTFSI electrolytes. Macromolecules **2010**, 43, 3502–3510.

(47) Vega, C.; Abascal, J. A general purpose model for the condensed phases of water: TIP4P/2005. J. Chem. Phys. **2005**, 123, 234505–1 – 234505–12.

(48) Zeron, I. M.; Abascal, J. L. F.; Vega, C. A force field of Li+, Na+, K+, Mg2+, Ca2+, Cl-, SO42- in aqueous solution based on the TIP4P/2005 water model and scaled charges for the ions. J. Chem. Phys. **2019**, 151, 134504.

(49) Joung, I. S.; Cheatham, T. E. I. Determination of alkali and halide monovalent ion parameters for use in explicitly solvated biomolecular simulations. J. Phys. Chem. B **2008**, 112, 9020–9041, PMID: 18593145.

(50) Horinek, D.; Mamatkulov, S. I.; Netz, R. R. Rational design of ion force fields based on thermodynamic solvation properties. J. Chem. Phys. **2009**, 130, 124507.

(51) Mazur, S. Neighborship partition of the radial distribution function for simple liquids. J. Chem. Phys. **1992**, 97, 9276–9282.

(52) Fukushima, T.; Matsuda, Y.; Hashimoto, H.; Arakawa, R. Solvation of lithium ions in organic electrolytes of primary lithium batteries by electrospray ionization-mass spectroscopy. J. Power Sources **2002**, 110, 34–37.

(53) Zheng, D.; Qu, D.; Yang, X.-Q.; Lee, H.-S.; Qu, D. Preferential solvation of lithium cations and impacts on oxygen reduction in lithium–air batteries. ACS Appl. Mater. Interfaces **2015**, 7, 19923–19929, PMID: 26301499.

(54) Ganesh, P.; Jiang, D.-e.; Kent, P. R. C. Accurate static and dynamic properties of liquid electrolytes for Li-ion batteries from ab initio molecular dynamics. J. Phys. Chem. B **2011**, 115, 3085–3090, PMID: 21384941.

(55) Tsuzuki, S.; Shinoda, W.; Matsugami, M.; Umebayashi, Y.; Ueno, K.; Mandai, T.; Seki, S.; Dokko, K.; Watanabe, M. Structures of [Li(glyme)]+ complexes and their interactions with anions in equimolar mixtures of glymes and Li[TFSA]: analysis by molecular dynamics simulations. Phys. Chem. Chem. Phys. **2015**, 17, 126–129.

(56) Chaudhari, M. I.; Nair, J. R.; Pratt, L. R.; Soto, F. A.; Balbuena, P. B.; Rempe, S. B. Scaling atomic partial charges of carbonate solvents for lithium ion solvation and diffusion. J. Chem. Theory Comput. **2016**, 12, 5709–5718, PMID: 27767309.

(57) Flores, E.; Åvall, G.; Jeschke, S.; Johansson, P. Solvation structure in dilute to highly concentrated electrolytes for lithium-ion and sodium-ion batteries. Electrochim. Acta **2017**, 233, 134–141.

(58) Yang, H.; Yin, L.; Shi, H.; He, K.; Cheng, H.-M.; Li, F. Suppressing lithium dendrite formation by slowing its desolvation kinetics. Chem. Commun. **2019**, 55, 13211–13214.

(59) Cui, W.; Lansac, Y.; Lee, H.; Hong, S.-T.; Jang, Y. H. Lithium ion solvation by ethylene carbonates in lithium-ion battery electrolytes, revisited by density functional theory with the hybrid solvation model and free energy correction in solution. Phys. Chem. Chem. Phys. **2016**, 18, 23607–23612.

(60) Borodin, O.; Olguin, M.; Ganesh, P.; Kent, P. R. C.; Allen, J. L.; Henderson, W. A. Competitive lithium solvation of linear and cyclic carbonates from quantum chemistry. Phys. Chem. Chem. Phys. **2016**, 18, 164–175.

(61) Rempe, S.; Pratt, L.; Hummer, G.; Kress, J.; Martin, R. L.; Redondo, A. The hydration number of Li^+ in liquid water. J. Am. Chem. Soc. **2000**, 122, 966–967.

(62) Petersen, G.; Jacobsson, P.; Torell, L. A Raman study of ion—polymer and ion—ion interactions in low molecular weight polyether—LiCF3SO3 complexes. Electrochim. Acta **1992**, 37, 1495–1497.

(63) Huang, W.; Frech, R. Dependence of ionic association on polymer chain length in poly(ethylene oxide)-lithium triflate complexes. Polymer **1994**, 35, 235–242.

(64) Frech, R.; Huang, W. Polymer conformation and ionic association in complexes of lithium, sodium and potassium triflate with poly (ethylene oxide) oligomers. Solid State Ionics **1994**, 72, 103–107.

(65) Sandner, B.; Tübke, J.; Wartewig, S.; Shashkov, S. Ionic association in oligo(ethylene glycol)-lithium triflat solutions as studied by FT Raman spectroscopy. Solid State Ionics **1996**, 83, 87–97.

(66) Lytle, T. K.; Muralidharan, A.; Yethiraj, A. Why lithium ions stick to some anions and not others. J. Phys. Chem. B **2021**, 125, 4447–4455, PMID: 33881867.

(67) Xu, K. Navigating the minefield of battery literature. Commun. Mater. **2022**, 3.

(68) Luzar, A.; Chandler, D. Effect of environment on hydrogen bond dynamics in liquid water. Phys. Rev. Lett. **1996**, 76, 928–931.

(69) Müller-Plathe, F. Microscopic dynamics in water-swollen poly(vinyl alcohol). J. Chem. Phys. **1998**, 108, 8252–8263.

(70) Chandra, A. Effects of ion atmosphere on hydrogen-bond dynamics in aqueous electrolyte solutions. Phys. Rev. Lett. **2000**, 85, 768–771.

(71) Zhao, W.; Leroy, F.; Heggen, B.; Zahn, S.; Kirchner, B.; Balasubramanian, S.; Müller-Plathe, F. Are there stable ion-pairs in room-temperature ionic liquids? Molecular dynamics simulations of 1-n-butyl-3-methylimidazolium jexafluorophosphate. J. Am. Chem. Soc. **2009**, 131, 15825–15833, PMID: 19827790.

TOC Graphic

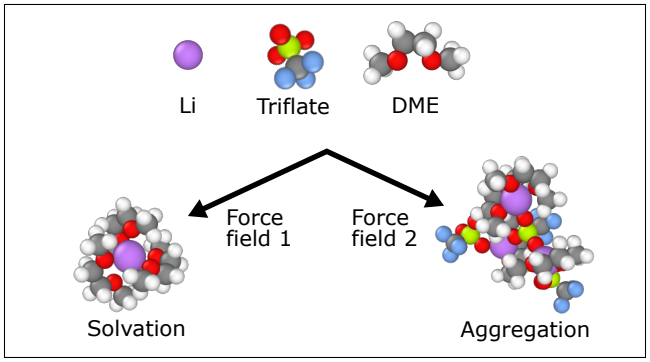
Li
Triflate
DME
Force
field 1
Force
field 2
Solvation
Aggregation